Effects of different boundary conditions on the long-range structure of polar liquids

2008 J. Phys.: Condens. Matter 20 494204

(http://iopscience.iop.org/0953-8984/20/49/494204)

IOP PUBLISHING JOURNAL OF PHYSICS: CONDENSED MATTER

J. Phys.: Condens. Matter **20** (2008) 494204 (9pp) doi:10.1088/0953-8984/20/49/494204

Effects of different boundary conditions on the long-range structure of polar liquids

Gunnar Karlström[1], Joakim Stenhammar[2] and Per Linse[2]

[1] Division of Theoretical Chemistry, Center for Chemistry and Chemical Engineering, Lund University, PO Box 124, S-221 00 Lund, Sweden
[2] Division of Physical Chemistry 1, Center for Chemistry and Chemical Engineering, Lund University, PO Box 124, S-221 00 Lund, Sweden

Received 30 July 2008, in final form 28 September 2008
Published 12 November 2008
Online at stacks.iop.org/JPhysCM/20/494204

Abstract

The long-range order in strongly coupled dipolar systems has been studied using large-scale simulations for systems containing up to 100 000 particles. It is found that the boundary conditions used strongly influence the result. It is found that a periodic system modeled with the minimum image approximation yields an artificial order, whereas the same system described using the Ewald summation technique is slightly less long-range ordered, as compared to the results obtained from studies on a non-periodical spherical droplet. Analytical expressions together with scaling considerations suggest that dipolar systems are structured on all length scales. However, more extensive studies are needed to fully assess the impact of using different boundary conditions on the long-range structure of polar liquids.

(Some figures in this article are in colour only in the electronic version)

1. Introduction

The packing of dipolar particles is a fundamental problem within physics and chemistry that is not fully understood when the dipolar interaction between the particles is larger than the thermal energy kT. The problem has been extensively studied, primarily with theoretical methods [1–35]. The reference list contains some of the latest and some of the more fundamental works, but for a more comprehensive review, the reader is referred to a preceding article [36]. The field has received increasing interest due to the recent experimental findings of Shelton [37–41], who suggests, based on scattering experiments, that ferroelectric domains with a long relaxation time, of the order of nanoseconds, are observed in dipolar liquids, provided that the dipole–dipole interaction is large enough. His findings have been questioned by Pounds and Madden, based on large-scale (28 000 particles) modeling of dipolar systems using periodic boundary conditions described using the Ewald summation technique [31]. On the other hand, the findings of Shelton have gained some support from the droplet simulations of similarly sized systems presented in our previous work, where ferroelectric domains were indeed observed, however with a much faster relaxation of the dipolar order [36].

The purpose of this work is to investigate if the discrepancy between the results obtained in these two previous studies can be understood, and if so, maybe something new can be learned from this. In the next section we will shortly examine some scaling properties of the dipolar interaction that could be of interest for our understanding of the behavior of dipolar systems.

2. Scaling considerations

The dipole–dipole interaction has a special position among the different types of interactions that may occur in uncharged systems since it is only conditionally convergent. By this we mean that the formal $1/r^3$ behavior of the interaction is only convergent if the potential is first averaged over all intermolecular angles.

A general property of a spherical volume in a liquid that must be fulfilled in order for the studied system to behave as a dielectric medium is that the average value of μ^2/V or μ^2/r^3, where μ is the dipole moment of the volume, V the size of the volume and r its radius, must be independent of V. Neumann [15] has shown that there is a unique relation between the dielectric permittivity of the liquid and the average values mentioned above. In particular he showed that if the studied system is surrounded by a medium with the same dielectric permittivity as that of the sphere, then the following

equation should hold

$$\langle \mu^2/V \rangle = \frac{kT}{4\pi}\frac{(\varepsilon-1)(2\varepsilon+1)}{\varepsilon}. \quad (1a)$$

If we instead assume that the surrounding medium has an infinite dielectric permittivity, as in the case of Ewald boundary conditions with conducting surroundings, the following relation should hold

$$\langle \mu^2/V \rangle = \frac{3kT}{4\pi}(\varepsilon-1). \quad (1b)$$

In these equations, ε is the relative dielectric permittivity of the medium and the bracket notation indicates a statistical–mechanical average.

One can use the Born model for the calculation of the solvation free energy of a dipole [42]. This model relates μ^2/r^3 to the solvation free energy of a system according to

$$G_{\text{solv}}(\mu) = -\frac{\varepsilon-1}{2\varepsilon+1}\frac{\mu^2}{r^3}. \quad (2)$$

If equations (1) and (2) are combined and we use the fact that the volume of a sphere equals $\frac{4\pi r^3}{3}$, we obtain

$$G_{\text{solv}}(\mu) = -\frac{(\varepsilon-1)^2}{3\varepsilon}kT \approx -\frac{\varepsilon}{3}kT \quad (3a)$$

and

$$G_{\text{solv}}(\mu) = -\frac{(\varepsilon-1)^2}{2\varepsilon+1}kT \approx -\frac{\varepsilon}{2}kT. \quad (3b)$$

Equation (3*a*) is valid when the permittivity of the surroundings is the same as that of the sphere, and (3*b*) holds when the permittivity of the surroundings is infinite. The last parts of the equations are valid for large ε. The results are, to our knowledge, new and they show that any volume large enough to behave as a dielectric medium is strongly coupled to its surroundings provided that the dielectric permittivity is large. In this work we focus on systems with relative permittivities of the order of 100. This means that the dipole moment in an arbitrarily sized volume is coupled to the surroundings with $\sim 30\ kT$. The average orientation of the surrounding dipoles is thus extremely well defined.

Since $\langle \mu^2/V \rangle$ is independent of the volume in a dielectric medium and N (the number of particles in the volume) is proportional to V, we may conclude that μ is proportional to $\sqrt{N}$. We may thus write $\langle \mu \rangle = a\sqrt{N}$, where a is a numerical constant independent of N. Formally we may thus write the average interaction $\langle E(\mu, \mu') \rangle$ between two equally large volumes at close contact as

$$\langle E(\mu, \mu') \rangle \propto a\sqrt{N}a\sqrt{N}/r^3 \propto a^2. \quad (4)$$

In this equation, $a\sqrt{N}$ is a measure of the dipole moment of the volumes and r is the distance between them. The last step in equation (4) is obtained by using the fact that $N \propto r^3$. The important issue is that this coupling exists on all length scales, and that dipolar liquids are consequently structured on all length scales.

To illustrate an interesting property of the dipolar interaction we may assume that the dipole moment of a volume was obtained by perfectly ordering all dipoles in the volume. It can easily be shown that the internal energy for such an arrangement is zero, apart from a small surface term. For this configuration we can write that $\mu = N\mu_0$, where μ_0 is the dipole moment of one particle. If we now use the configurations generated by a simulation applying periodic boundaries and the Ewald summation, using the original particles with dipole moment μ_0, but replace these particles with 'pseudo-particles' having the dipole moment $N\mu_0$, and scale the length scale of the system by a factor $N^{1/3}$, then the energy for this new system, which contains N times as many particles in the simulation box as the original system, will be exactly N times the energy obtained for the original system. This means that the energy per particle will be the same in the two systems.

We may thus conclude that we can obtain the total interaction energy in a dipolar system by creating order at any length scale, although the entropic cost, and thus the free energy, will be different.

3. Model and methods

3.1. Model

We consider a model system composed of N particles in a cubic volume V at a temperature T. The potential energy U of the system is assumed to be pairwise additive according to

$$U = \sum_{i=1}^{N-1}\sum_{j=i+1}^{N} u_{ij}(r_{ij}). \quad (5)$$

The interaction between molecules i and j, u_{ij}, is composed of a Lennard-Jones (LJ) and a dipole–dipole potential (also referred to as a Stockmayer potential) according to

$$u_{ij}(r_{ij}) = u_{ij}^{\text{LJ}}(r_{ij}) + u_{ij}^{\text{dip}}(r_{ij}) \quad (6)$$

with

$$u_{ij}^{\text{LJ}}(r_{ij}) = 4\varepsilon\left[\left(\frac{\sigma}{r_{ij}}\right)^{12} - \left(\frac{\sigma}{r_{ij}}\right)^{6}\right] \quad (7)$$

$$u_{ij}^{\text{dip}}(r_{ij}) = \frac{1}{4\pi\varepsilon_0}\left[\frac{\boldsymbol{\mu}_i \cdot \boldsymbol{\mu}_j}{r_{ij}^3} - \frac{3(\boldsymbol{\mu}_i \cdot \mathbf{r}_{ij})(\boldsymbol{\mu}_j \cdot \mathbf{r}_{ij})}{r_{ij}^5}\right] \quad (8)$$

where the size parameter σ and interaction parameter ε characterize the LJ interaction, $\boldsymbol{\mu}_i$ denotes the dipole vector of particle i, $\mathbf{r}_{ij}$ is the vector between particle i and j, and $r_{ij} = |\mathbf{r}_{ij}|$.

In this study, we have used the LJ parameters $\sigma = 2.8863$ Å and $\varepsilon = 1.970\,23$ kJ mol^{-1}. The dipole strengths were equal to $\mu = |\boldsymbol{\mu}| = 0.105\,84$, 0.238 13, and 0.343 97$e$ Å. The number density was held fixed at $\rho = 0.038\,446$ Å^{-3} and the temperature at $T = 315.8$ K. The number of particles ranged from $N = 1000$ to 100 000. The parameters of the system with the largest dipole moment ($\mu = 0.343\,97e$ Å) were chosen so as to model a system with long-range properties similar to those of water and close to those in [22] and [36]. In reduced units the systems are characterized by $\rho^* = \rho\sigma^3 = 0.9244$, $T^* = kT/\varepsilon = 1.333$, and $\mu^* = \mu/(4\pi\varepsilon_0\varepsilon\sigma^3)^{1/2} = 0.5732$, 1.290, and 1.863.

Table 1. Number of particles, box length, and the truncation in the real and reciprocal spaces of the Ewald summation for the systems investigated.

		Ewald summation	
N	L (Å)	R_{cut} (Å)	n_{cut}
1 000	29.629	14	7
3 000	42.732	14	9
10 000	63.833	19	11
30 000	92.063	21	15
100 000	137.52	27	15

3.2. Simulation aspects

The properties of the model systems were determined by performing molecular dynamics (MD) simulations at constant number of particles, volume, and temperature. The particles were enclosed in a cubic box with length L, and periodical boundary conditions were applied. Table 1 provides the box lengths used.

The long-range dipole–dipole interactions were treated using two different schemes: (i) the Ewald summation adapted to dipolar systems [44] using conducting boundary conditions and (ii) the minimum image (MI) convention. The former approach formally involves an infinite periodic system where the dipole–dipole interaction energy is divided into several terms. The latter approach considers the interaction between a dipole and its nearest image after considering the periodic boundary conditions [45]. An Ewald convergence parameter $\alpha = 3.2/R_{\text{cut}}$ was used in conjunction with the spherical cutoff distance R_{cut} in real space and the spherical cutoff n_{cut} in reciprocal space given in table 1. The LJ interactions were subjected to (i) the same spherical cutoff as the dipole–dipole interaction in real space (Ewald summation) and (ii) the same truncation as the dipole–dipole interaction (MI convention). Hence, the spherical cutoff distance of the LJ interactions depended on the boundary conditions and the system size. However, even for the smallest system size, $R_{\text{cut}} \approx 14 \approx 3.5\sigma$, making the effect on the structure of the cutoff of the LJ interaction negligible.

The MD simulations were performed using the velocity Verlet algorithm with the orientations described by quaternions using a time step $\Delta t = 0.001$ ps, corresponding to a reduced time step $\Delta t^* = \Delta t/(m\sigma^2/\varepsilon)^{1/2} = 0.0011$, where the mass $m = 18$ g mol^{-1} has been used. The particles were treated as spherical tops with the components of the moment of inertia $I_{xx} = I_{yy} = I_{zz} = 1$ gÅ^2 mol^{-1}. If nothing else is stated, a simulation involved 10^5 time steps, hence extending over $t_{\text{sim}} = 100$ ps or 115 reduced time units. In some cases, 10-fold longer simulations were performed. Berendsen's [47] approach of coupling the system to an external bath to preserve the temperature was used, with a time coupling constant of $100\Delta t$. This weak coupling only suppresses the potential energy drift and does not affect the relevant dynamics of the system.

The reported uncertainties are one standard deviation and were evaluated by subdividing the production runs into 10 sub-batches. The integrated Monte Carlo/molecular dynamics/Brownian dynamics simulation package MOLSIM [46] for molecular systems was employed throughout.

For comparison we will also present data obtained for droplets of dipolar particles with vacuum surroundings. The technical aspects of these simulations have been fully described elsewhere [36]. Apart from the droplet results presented in the earlier publication, we will also present some new results obtained for a larger droplet system containing 60 000 particles. The parameters describing the particles of the droplets are the same as those of the simulations described above, and the volume per particle is close to 26.0 Å^3.

3.3. Domain and volume dipole moment analyses

One of the most important issues of the present investigation is the formation of ferroelectric domains. In this analysis, our point of departure is the degree of ordering of the directions of the dipoles in a spherical volume V with radius R centered on dipole i according to

$$\widehat{G}_{k,i}(R) = \frac{1}{\mu^2}\left(\boldsymbol{\mu}_i \cdot \sum_{j\in V}\boldsymbol{\mu}_j\right). \tag{9}$$

If the dipoles in V are orientationally uncorrelated, $\widehat{G}_{k,i}(R) = 1$, whereas if they are positively correlated $\widehat{G}_{k,i}(R) > 1$, and if they are negatively correlated $\widehat{G}_{k,i}(R) < 1$. The time average of $\widehat{G}_{k,i}(R)$ will be denoted $G_{k,i}(R)$. Moreover, for a homogeneous system, we can average $G_{k,i}(R)$ over all the particles according to

$$G_k(R) = \frac{1}{N}\sum_{i=1}^{N} G_{k,i}(R) \tag{10}$$

which is often referred to as the distance dependent Kirkwood factor [32]. If the summation in equation (10) extends over a sufficiently large volume such that all correlations with the central particle are included and the size of the studied system is much larger than this volume, the Kirkwood factor g_k is obtained according to

$$\begin{aligned} g_k &= \lim_{R_{\text{sys}}/R\to\infty}\lim_{R\to\infty} G_k(R) \\ &= \lim_{R_{\text{sys}}/R\to\infty}\lim_{R\to\infty}\frac{1}{\mu^2}\frac{1}{N}\sum_{i=1}^{N}\left(\overline{\boldsymbol{\mu}_i \cdot \sum_{j\in V}\boldsymbol{\mu}_j}\right). \end{aligned} \tag{11}$$

It should be noted that there is an underlying assumption that the correlations in the liquid do not have infinite range, since then the Kirkwood factor g_k lacks meaning. Nevertheless, for each configuration the degree and extension of the dipole ordering around all particles were determined. The first nontrivial maximum of $\widehat{G}_{k,i}(R)$, $\widehat{G}_{k,i}^{\max}$, was used as a measure of the strength of the dipole ordering around particle i and the radius at which $\widehat{G}_{k,i}(R)$ displayed its first maximum, $R_{\max,i}$, as the measure of the extension of this region of ordered dipoles. A maximum was considered as being nontrivial if it was followed by a decaying $\widehat{G}_{k,i}(R)$ for at least three histogram

Table 2. Total, LJ, and dipole potential energy at different dipole strength, boundary conditions and number of particles.

μ (e Å)	Boundary condition	N	U (kJ mol^{-1})		U_{LJ} (kJ mol^{-1})		U_{dip} (kJ mol^{-1})	
0.105 84	Ewald	1 000	−11.511	0.004	−11.197	0.004	−0.314	0.002
		3 000	−11.553	0.002	−11.243	0.002	−0.310	0.001
		10 000	−11.590	0.001	−11.280	0.001	−0.310	0.001
		30 000	−11.598	0.001	−11.287	0.001	−0.311	0.001
	MI	1 000	−11.572	0.004	−11.259	0.004	−0.312	0.002
		3 000	−11.622	0.002	−11.313	0.002	−0.310	0.001
		10 000	−11.641	0.002	−11.332	0.002	−0.309	0.001
		30 000	−11.654	0.001	−11.345	0.001	−0.309	0.001
0.238 13	Ewald	1 000	−15.262	0.003	−10.967	0.004	−4.294	0.004
		3 000	−15.304	0.003	−11.015	0.003	−4.290	0.003
		10 000	−15.339	0.002	−11.050	0.001	−4.289	0.002
		30 000	−15.345	0.002	−11.060	0.001	−4.285	0.002
		100 000	−15.374	0.002	−11.090	0.001	−4.284	0.001
	MI	1 000	−15.394	0.007	−11.038	0.005	−4.356	0.005
		3 000	−15.428	0.005	−11.087	0.002	−4.340	0.004
		10 000	−15.418	0.002	−11.105	0.001	−4.313	0.002
		30 000	−15.414	0.002	−11.117	0.001	−4.297	0.002
0.343 97	Ewald	1 000	−22.243	0.006	−10.380	0.005	−11.863	0.007
		3 000	−22.286	0.004	−10.426	0.002	−11.861	0.004
		10 000	−22.317	0.002	−10.461	0.001	−11.856	0.002
		30 000	−22.325	0.002	−10.469	0.001	−11.856	0.002
		100 000	−22.355	0.001	−10.502	0.001	−11.854	0.001
	Ewald, $\varepsilon = 1$	30 000	−22.328	0.002	−10.469	0.001	−11.858	0.002
	MI	1 000	−24.30	0.02	−10.539	0.004	−13.76	0.02
		3 000	−24.657	0.008	−10.623	0.002	−14.034	0.009
		10 000	−24.830	0.002	−10.658	0.001	−14.172	0.003
		30 000	−24.907	0.003	−10.675	0.001	−14.232	0.003
	Droplet	1 000	−19.678	0.03	−8.625	0.01	−11.292	0.02
		3 000	−19.941	0.07	−9.260	0.02	−11.668	0.03
		10 000	−21.417	0.04	−9.749	0.02	−11.944	0.03
		30 000	−21.869	0.04	−10.061	0.02	−12.101	0.03
		60 000	−22.128	0.08	−10.231	0.04	−12.239	0.07

bins, each of them with a width of 0.20 Å, an approach which should filter out statistical fluctuations. From $\widehat{G}_{k,i}^{\max}$ ($i = 1, \ldots, N$), a set of domains containing particles with correlated dipole directions was constructed as follows: A search was made for the particle with the largest value of $\widehat{G}_k^{\max}$. The sphere with radius $R_{\max}$ centered at this particle was considered as being a domain. The particles inside this domain were excluded from further searches. The search was then repeated among the remaining (nonexcluded) particles. The search for ferroelectric domains was (arbitrarily) stopped (i) if $\widehat{G}_k^{\max}$ became less than 50% of $\widehat{G}_k^{\max}$ of the first domain or (ii) after identification of 20 domains. It should be noted that by this approach the domains are not necessarily spatially nonoverlapping.

A quantity that is closely linked to the domains is the dipole moment of a fixed volume. Kusalik [43] has shown that the dipole moment probability distribution of a spherical volume with radius r in a liquid should obey the simple relation

$$P(\mu) = A\mu^2 \, \mathrm{e}^{-\alpha\mu^2/r^3} \tag{12}$$

where α is a constant that only depends on the dielectric permittivity of the medium in the droplet and in the surroundings, and A is a normalization constant. Below we will present such distributions, whose appearance will reveal interesting properties of the studied systems.

4. Results

4.1. Energetics

The potential energy U of the system, the LJ potential energy U_{LJ} and the dipole–dipole potential energy U_{dip} at different dipole strengths, boundary conditions, and system sizes are given in table 2. In this table we also present the corresponding data obtained from Monte Carlo simulations [36] of the same particles under similar conditions in a droplet using the largest of the three dipole moments. The most interesting observations obtained using the MI convention and the Ewald summation are analyzed as follows:

(i) At increasing dipole strength, U_{LJ} becomes slightly less negative, whereas the magnitude of U_{dip} increases faster than μ^2. At the largest value of μ, the values of U_{LJ} and U_{dip} are comparable.
(ii) The MI convention produces a more negative U_{LJ} and a more negative U_{dip} as compared to the Ewald summation.
(iii) With the MI convention, U_{dip} displays a system-size dependence that increases with μ, whereas with the Ewald

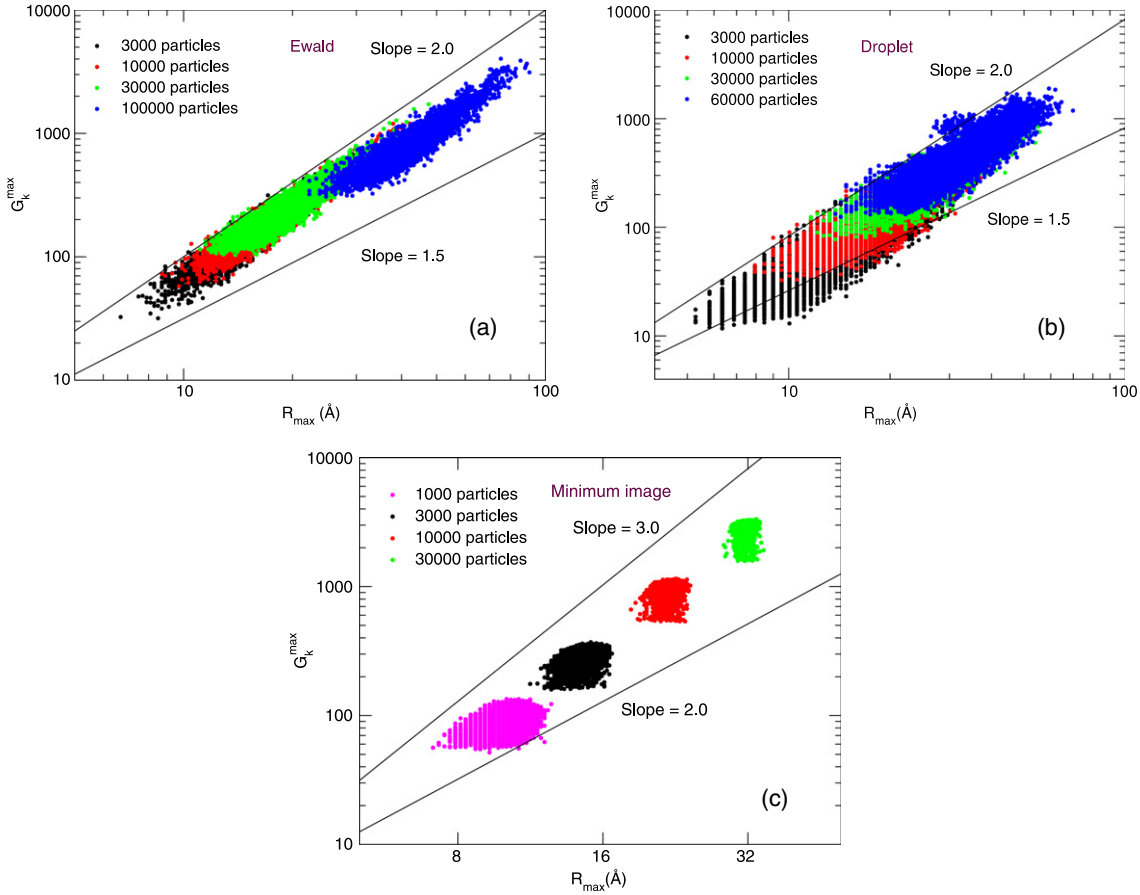

Figure 1. Maximum Kirkwood factor $\widehat{G}_k^{\max}$ versus the domain radius $R_{\max}$ in a log–log representation for systems treated with (a) Ewald summation, (b) a spherical droplet, and (c) the minimum image convention.

summation the corresponding system-size dependence is negligible.

(iv) With the two smaller values of μ, U_{dip} extrapolated to $N \to \infty$ converges to the same value for the two boundary conditions, but with the largest μ the extrapolated values differ from each other by 20%.

No energetic comparison is made with the droplet simulations, since the presence of the surface influence the droplet energetics significantly. We will just briefly mention that the energetics of the droplet are similar to those of the Ewald boundary system.

4.2. Structure

It is standard in these types of studies to characterize the short-range structure around a dipolar particle. We have also done this in the present study, but the results are similar to those reported elsewhere [22, 23] and will not be presented here. Moreover, we do not find any significant differences between the Ewald results and the droplet results as far as the short-range structure is concerned. We will therefore focus only on the long-range solvation properties. These will shed some light on the influence of the different boundary conditions used in this study, but also on the general properties of dipolar liquids. To illuminate these issues we have chosen to present three different types of data: (i) information about domain size and the maximum Kirkwood factor as a function of the boundary condition and the number of particles in the system, (ii) dipole moment probability distribution functions and (iii) the effective particle–particle interaction energy as a function of particle separation.

4.2.1. Domain size distributions. In figure 1 we present scatter plots showing the relation between the size of the domains and their maximum Kirkwood factor, identified by the procedure outlined in the methods section. Each data point in the figures represents the size and magnitude of the first identified domain of each configuration. The data presented in figure 1(a) was obtained using the Ewald summation, figure 1(b) presents the droplet data and figure 1(c) shows data obtained using MI convention. In each figure two lines are inserted to help the eye identify the slope of the distributions. From arguments given above one should expect that a liquid exhibiting dielectric properties would yield a slope of 1.5 in the logarithmic plots, corresponding to $\mu \propto r^{3/2}$. For each boundary condition four different systems with different numbers of particles are presented.

The most striking feature is the very different behavior of the MI system, presented in figure 1(c), compared to the other two systems. The slope observed here is close to 2.5, indicating a strong non-dielectric behavior. Furthermore, it is clear that the maximum Kirkwood factor versus domain size

distributions become more localized as the size of the system grows. It also deserves to be said that in almost all of the configurations generated using the MI convention the domain identification procedure finds between 14 and 17 domains, whereas the spread in the observed number of domains using the other two boundary conditions is larger. If we calculate the alignment of the dipoles in the identified domains, that is the observed maximum Kirkwood factor divided by the number of particles inside the spherical domain for the domain with the largest value of $\widehat{G}_k^{\max}$ in each configuration, we typically obtain values between 0.1 and 0.25, where the larger values are obtained for the larger systems. This indicates that we are observing a system that gets more and more structured as its size increases. For the system containing 10 000 particles, the time correlation function for the dipole vector of the largest domains remains at a value of $\approx$1 during the whole time window of the statistical evaluation (2.0 ps). It is thus reasonable to characterize the system as frozen on the length scale of the domains. What has happened is that the system has adopted configurations where a large part of the interaction energy is obtained at the length scale of the domains (30–40 Å). The reason for this is that by this type of structuring it is possible to localize domains with repulsive interactions outside the MI box. The effect becomes more pronounced when the size of the system grows, and it is possible to form structures with large dipole moments without severely disrupting the short-range dipole–dipole interaction. We thus see that the MI convention generates an unphysical behavior of the studied system. This has been said many times before, and we will focus the remaining part of this study on the two other types of boundary conditions.

If we now focus on the other two systems, we see that the scatter plots indicate that the relation between μ and r corresponds to a slope between 1.5 and 2. For the droplet system a larger number of particles seems to imply a somewhat larger slope, whereas the opposite is true for the Ewald system where the largest system seems to approach a slope of 1.5. We also see that the spread in the data is more pronounced for the droplets than for the Ewald system. It seems reasonable to assume that this is an effect of the fact that different parts of the droplets have different surroundings, whereas the Ewald system is homogeneous. The first difference is, however, more difficult to understand and we will return to this issue in the discussions of the next two subsections.

4.2.2. Fixed volume dipole moment distributions. In this subsection we will look into the probability distributions for the dipole moment of a fixed volume, and compare our results to the theoretically predicted functional form of equation (12).

The data that we will present here is the dipole moment distribution for a fixed spherical volume centered at an arbitrary particle in the system. For the droplet system this approach may present problems, since not all dipoles are surrounded by a sphere with a given radius that is filled with particles. Moreover, the relative dielectric permittivity of the region outside the droplet is equal to 1, whereas volumes in the inner part of the droplet are surrounded by a thinner or thicker layer of liquid with a higher dielectric permittivity. For the volumes located in the Ewald system the situation is more or less the opposite, since all spheres are full of dipoles and the dielectric permittivity at long distances is infinite. Considering these problems, one would perhaps consider it meaningless to compare the different curves obtained, but we still claim it to be meaningful, which will be explained below. The data that we will present in this and in the following subsection was obtained for the two largest studied systems (an Ewald system with 100 000 particles and a droplet with 60 000 particles). In figures 2(a) and (b) we present probability distribution functions describing the normalized dipole moment probabilities for the different systems and for spherical volumes of different radii. In figure 2(a) we present Ewald boundary condition data and in figure 2(b) we present the results from the droplet system. The different curves correspond to different radii, varying between 10 and 60 Å. To make the curves comparable, the dipole moments have been scaled with $1/r^{3/2}$, where r is the radius of the considered volume. To guide the eye, a curve with $\alpha = 0.5$ has been inserted in both figures. This corresponds to the distribution that would be obtained in a bulk system with a relative permittivity close to 90.

The following observations can be made from figure 2(a): (i) all the presented curves have a shape similar to that of the theoretical curve, and (ii) the curves obtained for larger volumes display larger normalized dipole moments. Two possible explanations can be given for the latter observation. Either the increase in the normalized dipole moment is a consequence of the dielectric response in the system gradually building up and that a larger sphere being needed to obtain a converged value, or the increase is due to the fact that the long-range response is characterized by the infinite dielectric permittivity used in the Ewald systems. A combination of these two effects is of course also possible.

If we look at figure 2(b) we see a different pattern. At the beginning the normalized dipole moments increase when the size of the sampled volume increases, but for larger volumes this increase becomes a decrease. The obvious explanation for this behavior is the same as for the Ewald system: an increasing number of volumes are empty when the size of the volumes increases, and the surrounding of the droplet has a low dielectric permittivity. Another more interesting observation can however be made, namely that the shape of the distribution does not follow the theoretical curve, in that enhanced probabilities for large dipole moments are found, as compared to the theoretical prediction. This is true for all the radii studied, but is best seen for the three smallest radii (10, 20 and 30 Å). To illustrate this we present the dipole moment distributions obtained for these radii in the droplet and Ewald systems in figure 2(c). In figure 2 it can clearly be seen that the maximum of the curves occurs at smaller dipole moments in the droplet, but that there is also a long tail with larger dipole moments present when using the droplet boundary. The interesting issue is whether these effects are also present in a real bulk liquid or if it is in some way induced by the surface and dies away as we depart from the surface. If the effect does exist in real bulk liquids, then the results obtained using the Ewald summation must be influenced by the implicit long-range structure induced by the periodicity in a similar way to

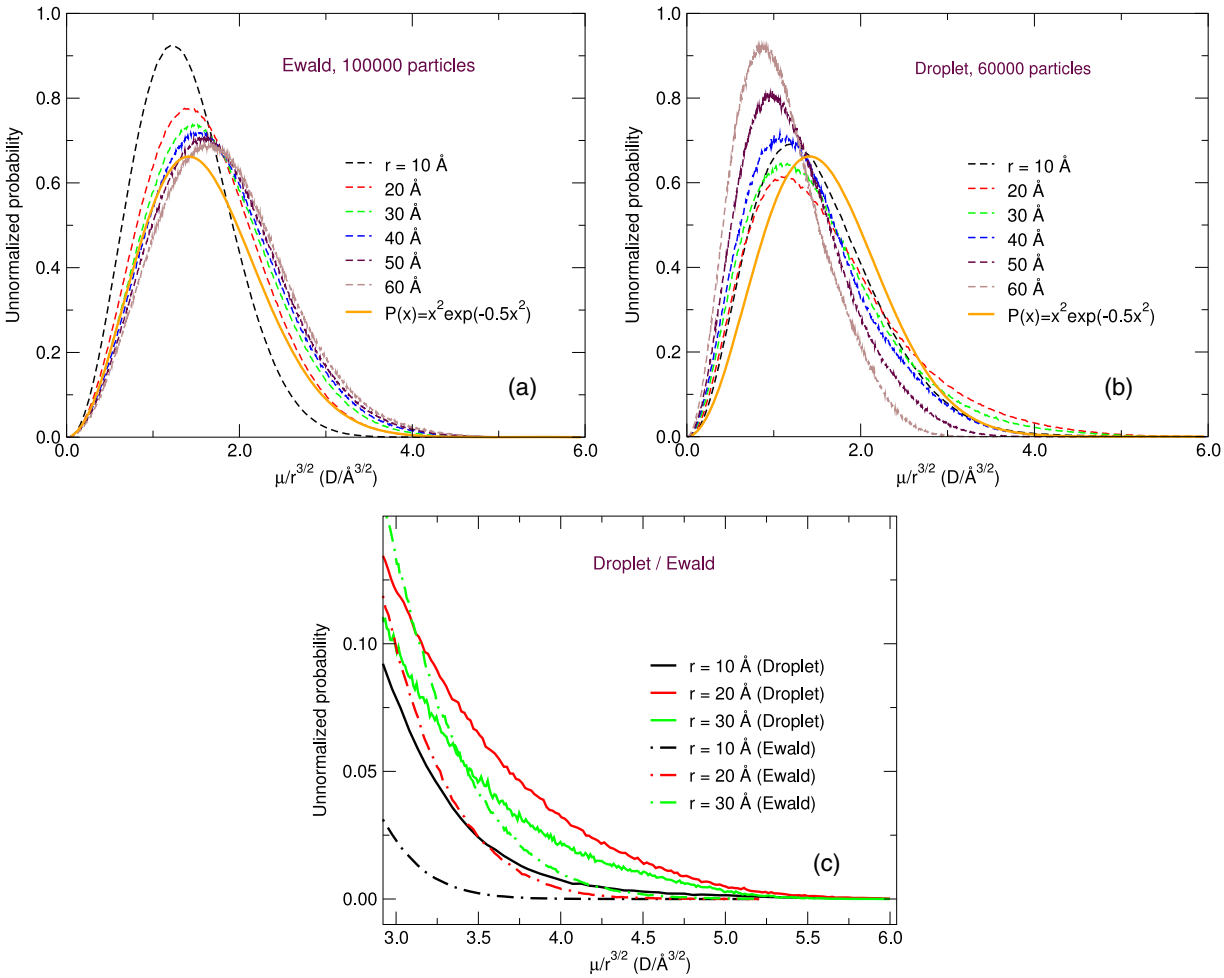

Figure 2. Scaled dipole moment distributions for spheres of different radii, obtained using (a) Ewald summation and (b) a spherical droplet. Panel (c) shows parts of the data from (a) and (b) using a different scale for clarity.

which the MI convention induced an enhanced structure. If so, the periodic boundary conditions destroy the build-up of long-range structure. In the next subsection we will look a bit further into this issue.

4.2.3. Effective particle–particle interaction. In the previous subsection we observed various degrees of long-range structure depending on the boundary conditions. Here we will look for an energetic origin of this structuring. For that purpose we present the particle–particle interaction calculated from the Ewald and droplet simulations. In figure 3 we present the average particle–particle interaction energy as a function of the particle–particle separation r. To show the distance dependence the two curves have been multiplied by r^5. There is a marked difference between the two curves outside 10–15 Å, in that for the Ewald system, the average particle–particle interaction decays as $1/r^6$ outside 15 Å, whereas for the droplet system, the curve shows a $1/r^5$ behavior to at least 30–35 Å. Outside 35 Å there is a region where the interaction decreases in magnitude, then there is a region between 45 and 55 Å where a clear $1/r^5$ dependence is seen once again. It should be noted that the statistical uncertainty in the region outside 35 Å is large for the droplet system [36]. Thus it cannot

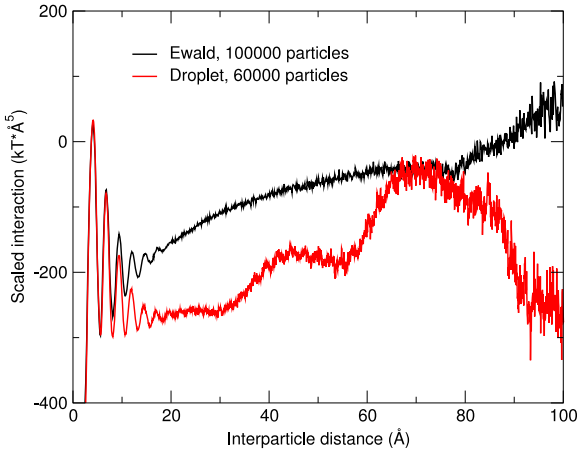

Figure 3. Scaled dipole–dipole interaction versus particle–particle separation for the largest Ewald and droplet systems.

be ruled out that the $1/r^5$-dependence region extends only to ∼30 Å, but it could equally well extend to separations of 55 Å. One could of course ask if there is a connection between the observed long-range energetics and the structuring discussed

above. The answer is most likely yes. If we consider a volume and assume that the dipole moment of volume is proportional to the square of its radius, then using the Born formula for the solvation free energy of a dipole, the equation (2), we see that this energy grows linearly with the volume radius. It is easy to show that this corresponds to an effective particle–particle interaction decaying as $1/r^5$.

5. Discussion and summary

We have seen in the previous section that there is a marked difference in the long-range structure of a truly periodic system made from dipolar particles with a large dipole–dipole interaction and that of a droplet composed of the same particles. We have also given scaling arguments indicating that this type of dipolar liquid is structured on all length scales. It is obvious that the assumption of a periodic system must influence the structuring on length scales that are comparable to the simulation box. It is equally obvious that the assumption of a spherical droplet explicitly defining the boundary may give an extra flexibility to the dipolar particles close to the surface. This extra flexibility may favor the formation of an increased dipolar order. Furthermore, from the MI data presented above it is clear that the seemingly obvious solution to make the studied system larger in no way guarantees a more correct behavior. In fact the formation of unphysical structures using the MI convention becomes more pronounced as the size of the system increases, as has been explained above.

One important question remains to be answered: which type of boundary condition should be preferred when modeling strongly coupled dipolar systems? To date the answer has been that one should prefer to model a periodic system using the Ewald summation technique. Based on the material presented here, there are reasons to doubt this. However, it is clear that more extensive studies are needed to fully understand the impact of using periodic or non-periodic boundaries on the structure of polar liquids.

We have seen that an arbitrary amount of the dipole–dipole interaction can be obtained at any length scale. What determines the actual amount of dipolar interaction energy that the system prefers to deliver at a particular length scale are the boundary conditions and the entropy cost that is associated with structuring the system at that length scale; in figure 2(c) we showed an increased structuring on the 10–30 Å length scale in the droplet systems, which is indeed in qualitative agreement with Shelton's findings [40]. It should, however, be noted that the timescale on which we have carried out our simulations (∼1 ns) is around two orders of magnitude shorter than the most slowly relaxing mode found by Shelton, which makes a direct comparison with the experimental results difficult. Furthermore, since we have shown that a dipolar system may indeed be structured on all length scales, it seems plausible that the very long relaxation times (∼50 ns) found by Shelton will only be observed in the 'true' thermodynamic limit, which is still far away from being reached using molecular simulations.

All systems that we deal with in real life have a surface. The question is thus if the structure imposed by the surface decays in regions that are distant form the surface or not. It is clear from the arguments given above that the structuring at the length scale of the simulation box can be influenced by the boundary in periodic systems. Is it possible that this influence of the boundary in turn influences the ordering at shorter length scales? It is further worth noting that we know for certain that the droplet systems will model the behavior of a real macroscopic system provided that it contains sufficiently many particles. We have also seen that the periodic system modeled using the MI convention will definitely not. The introduction of an artificial boundary condition, as in the Ewald systems, may induce an erroneous convergence behavior. It is thus appropriate to ask the question if a truly periodic system will converge to the same macroscopic system as the droplet and a real system. We will finish this report by saying that all aspects of dipolar systems are not fully understood, and that the long-ranged structure of such systems is highly dependent on the choice of simulation techniques used.

Acknowledgments

Financial support by the Swedish Research Council (VR) through the Linnaeus grant for the Organizing Molecular Matter (OMM) center of excellence and generous computer time at LUNARC as well as at the National Supercomputer Center (NSC) are gratefully acknowledged.

References

[1] Clausius R 1879 *Die Mechanische Wärmetheorie* vol II (Braunschweig: Vieweg Verlag) p 62
[2] Mossotti O F 1847 *Bibl. Univ. Modena* **6** 193
[3] Langevin P 1905 *Ann. Chim. Phys.* **5** 70
[4] Onsager L 1936 *J. Am. Chem. Soc.* **58** 1486
[5] Nienhuis G and Deutch J M 1971 *J. Chem. Phys.* **55** 4213
[6] Nienhuis G and Deutch J M 1972 *J. Chem. Phys.* **56** 235
[7] Nienhuis G and Deutch J M 1972 *J. Chem. Phys.* **56** 1819
[8] Wertheim M S 1973 *Mol. Phys.* **25** 211
[9] Wertheim M S 1973 *Mol. Phys.* **26** 1425
[10] Wertheim M S 1977 *Mol. Phys.* **33** 1109
[11] Wertheim M S 1979 *Annu. Rev. Phys. Chem.* **30** 471
[12] Ladd A J C 1977 *Mol. Phys.* **33** 1039
[13] Ladd A J C 1978 *Mol. Phys.* **36** 463
[14] Adams D J and McDonald I R 1976 *Mol. Phys.* **32** 931
[15] Neumann M 1983 *Mol. Phys.* **50** 841
[16] Levesque D, Patey G N and Weis J J 1977 *Mol. Phys.* **34** 1077
[17] Adams D J, Adams E M and Hills G J 1979 *Mol. Phys.* **38** 387
[18] Adams D J 1980 *Mol. Phys.* **40** 1261
[19] Adams D J 1981 *Mol. Phys.* **42** 907
[20] Neumann M, Steinhauser O and Pawley G S 1984 *Mol. Phys.* **52** 97
[21] Neumann M 1987 *Mol. Phys.* **60** 225
[22] Kusalik P G 1990 *J. Chem. Phys.* **93** 3520
[23] Kusalik P G 1991 *Mol. Phys.* **73** 1349
[24] Fröhlich H 1958 *Theory of Dielectrics* 2nd edn (Oxford: Clarendon)
[25] Berendsen H J C 1972 Molecular dynamics and Monte Carlo calculations on water *CECAM Report*
[26] Powles J G, Fowler R F and Evans W A B 1984 *Chem. Phys. Lett.* **107** 280
[27] Senapati S and Chandra A 2001 *J. Phys. Chem.* B **105** 5106
[28] Groh B and Dietrich S 1997 *Phys. Rev.* E **55** 2892
[29] Groh B and Dietrich S 1997 *Phys. Rev. Lett.* **79** 749

[30] Groh B and Dietrich S 1998 *Phys. Rev.* E **57** 4535
[31] Pounds M A and Madden P A 2007 *J. Chem. Phys.* **126** 104506
[32] Kirkwood J G 1939 *J. Chem. Phys.* **7** 911
[33] Ballenegger V and Hansen J-P 2005 *J. Chem. Phys.* **122** 114711
[34] Blaak R and Hansen J-P 2006 *J. Chem. Phys.* **124** 144714
[35] Wang Z, Holm C and Muller H W 2003 *J. Chem. Phys.* **119** 379
[36] Karlström G 2007 *J. Phys. Chem.* B **111** 10745
[37] Shelton D P 2005 *Phys. Rev.* B **72** 020201
[38] Shelton D P 2002 *J. Chem. Phys.* **117** 9374
[39] Shelton D P 2004 *J. Chem. Phys.* **121** 3349 (erratum)
[40] Shelton D P 2005 *J. Chem. Phys.* **123** 084502
[41] Shelton D P 2005 *J. Chem. Phys.* **123** 111103
[42] Israelachvili J 1996 *Intermolecular and Surface Forces* (New York: Academic)
[43] Kusalik P G 1993 *Mol. Phys.* **80** 225
[44] Ewald P 1921 *Ann. Phys.* **64** 253
[45] Frenkel D and Smit B 1996 *Understanding Molecular Simulation* (New York: Academic)
[46] Linse P 2007 *MOLSIM* (Sweden: Lund University)
[47] Berendsen H J C, Postma J P M, van Gunsteren W F, DiNola A and Haak J R 1984 *J. Chem. Phys.* **81** 2684